Carbon quantum dots as drug carriers for tumor-associated macrophage repolarization following photothermal therapy

Haizhong Yuan[a,†]**, Hui Yang**[b,†]**, Pin Yuan**[c]**, Tingting Wang**[d]**, Quan Zhou**[c,*]

[a] Pharmacy Department of PKU Care Lu'an Hospital, Shanxi 046204 China
[b] Department of Public Health and Preventive Medicine, Changzhi Medical College, Shanxi 046000 China
[c] Nanjing Jiatong Micro-nano Technology Co., Ltd., Jiangsu 210000 China
[d] Nanjing Seth Technology Service Co., Ltd., Jiangsu 210043 China

*Corresponding author, e-mail: 2262691619@qq.com
† These authors contributed equally to this work.

ABSTRACT: With the development of nanotechnology in the anticancer application, photothermal therapy (PTT) based on nanoparticles (NPs) could repolarize the tumor-associated macrophages (TAMs) from protumor (M2) phenotype to antitumor (M1) phenotype, thus regulating the tumor-suppressive immune environment. However, the inevitable local inflammation occurred in the residual tumor microenvironment after PTT recruited abundant abnormal TAMs to induce immune escape and survival of the remaining tumor cells. Here, TMP195 loaded carbon quantum dots (CQDs@TMP195) were developed as innovative nanoplatforms to achieve promising PTT and immune responses. In the nanoplatforms, CQDs with distinct antitumor performance were applied as an ideal drug-loading nanocarrier and initiated photothermal effects to generate heat under near-infrared (NIR) irradiation. The loaded TMP195 could repolarize the M2 phenotype TAMs into the M1 phenotype TAMs. Based on our work, the *in vitro* antitumor effects implied that CQDs@TMP195 could significantly kill cancer cells with minimal toxicity to normal cells. This study proposes a feasible therapeutic strategy for polarizing TAMs to the immunocompetent M1 phenotype after PTT.

KEYWORDS: photothermal therapy, tumor-associated macrophages, carbon quantum dots, immunocompetent M1 phenotype

INTRODUCTION

Compared to traditional anticancer strategies such as surgery, radiotherapy, and chemotherapy, phototherapy (e.g., photothermal therapy (PTT) and photodynamic therapy (PDT)) has been drawing growing attention due to the noninvasive and stimuli-responsive features [1–3]. As a light-triggered modality for cancer therapy, PTT is considered an ideal method, which possesses high therapeutic accuracy and low side effects [4, 5]. However, most of the existing PTT agents utilize visible light as an excitation source, which limits tissue penetration depth and induces severe photo-toxicity [6]. Hence, reducing the laser irradiation power of PTT would be highly desirable for its clinical applications.

The properties of photoluminescent carbon quantum dots (CQDs) such as excellent optical properties, high stability, water solubility, and good biocompatibility endow their advantages over conventional quantum dots and organic dyes [7–9]. Various types of research show that CQD properties are of great scientific interest in broadening their potential applications. For example, CQDs have been reported as promising bioimaging agents in biomedical applications due to their excellent photoluminescence properties [10, 11]. The surface functionalization of CQDs is suitable to serve as drug-delivery carriers and multifunctional

biomedicines against cancer [12]. Meanwhile, CQDs can be taken up by cells more easily and quickly, which is beneficial for drug delivery [13]. To broaden the application of CQDs in cancer therapy, CQDs should have strongly absorb light capability in the near-infrared region (NIR) in the wavelength range of 650–950 nm [14]. As reported, high tissue penetration can be achieved without damaging the surrounding normal tissues because of the low absorptivity of most normal tissue chromophores in the NIR region [15]. However, the application of CQDs in PTT is still limited as the main absorption area of CQDs is distributed in the ultraviolet (UV) range.

Tumor-associated macrophages (TAMs), one of the main tumor-infiltrating immune cells, play an important role in tumor development and prognosis [16, 17]. TAMs can be educated by the tumor microenvironment into different phenotypes. M1 phenotype TAMs exert antitumor activity by directly killing and phagocytosing tumor cells and inducing Th1-type immune response, while M2 phenotype TAMs can promote tumor growth, angiogenesis, and metastasis and inhibit T cell-mediated antitumor immunity [18–20]. Therefore, reprogramming M2 phenotype TAMs into M1 phenotype represents a potential cancer therapeutic approach [21–23]. A large number of M2 phenotype TAMs in the tumor microenvironment occur due to the chemotaxis of inflammatory cytokines after PTT

[24, 25]. Herein, the reduction of M2 phenotype TAMs would benefit remodeling the inflammatory immuno-suppressive microenvironment after PTT and further promote completely eliminating the residual tumor cells and preventing tumor recurrence.

In this work, CQDs with an absorption peak centered at 800 nm were facilely developed using a solvothermal method. Then, the TAM repolarization agent TMP195 was loaded onto the CQDs to form CQDs@TMP195. As photothermal transduction agents, CQDs can effectively convert laser in NIR to heat and ablate cancer cells. More importantly, the loaded TMP195 would significantly transform the M2 phenotype TAMs into M1 phenotypes [26]. Based on our results, CQDs@TMP195 showed relatively low cytotoxicity and great biocompatibility. The repolarization of TAMs effectively remodeled the immunosuppressive microenvironment in the residual tumor cell area after PTT (Fig. 1). Taken together, we fabricated innovative CQDs@TMP195 to enhance cancer therapy by initiating PTT and TAMs repolarization.

MATERIALS AND METHODS

Materials

All chemical reagents were of analytical grade and used without further purification. Dopamine hydrochloride (DA) was purchased from Sigma-Aldrich (USA). Dimethyl sulfoxide (DMSO, > 99.8%) and dialysis membranes (MWCO 1000 Da) were supplied by Sangon Biotech (Shanghai, China). Dulbecco's modification Eagle medium was attained from Hyclone (USA). Fetal bovine serum was purchased from Biological Industries (Israel). HeLa cells and macrophages (RAW264.7 cells) were provided by American Type Culture Collection (ATCC).

Instrumentation and characterization

UV-vis spectra were characterized by Perkin Elmer Lambda 750 UV-vis near-infrared spectrophotometer (UV-vis-NIR, Perkin-Elmer, USA). Diameter distribution and zeta potential were performed by Mastersizer2000 (DLS, Nano-ZS, UK). Morphology and diameter were represented by transmission electron microscopy (TEM, Tecnai G, Hong Kong). The laser of 808 nm was administrated by a power-tunable infrared laser (Laserwave, China).

Preparation of CQDs

Firstly, 50 mg DA was completely dissolved in 10 ml Tris buffer (10 mM, pH 8.5) and self-polymerized at room temperature for 2 h under magnetic stirring. Then, CQDs were synthesized by directly mixing 6 ml pre-polymerized polydopamine (PDA) solution and 20 ml glycerin (> 99%) and heated at 200 °C for 12 h in an autoclave. Finally, CQDs were purified via dialysis against DI water for 48 h (MWCO 1000 Da) and collected by centrifugation and lyophilization.

Loading of TMP195

A CQDs aqueous solution was mixed with TMP195 at different weight ratios and stirred at 600 rpm at 4 °C overnight. CQDs@TMP195 were then collected by centrifugation at 15,000 rpm for 20 min and washed 3 times to remove free TMP195. To determine the drug encapsulation efficiency and loading efficiency, CQDs@TMP195 were washed with acetonitrile 3 times, and the washing liquid was collected. The amount of TMP195 in the acetonitrile was quantified by high-performance liquid chromatography. The drug encapsulation efficiency and drug loading efficiency were calculated as follows: encapsulation efficiency (%) = mass of drug encapsulated in CQDs@TMP195/initial mass of drug × 100; loading efficiency (%) = mass of drug encapsulated in CQDs@TMP195/total mass of CQDs@TMP195 × 100.

Photothermal performance of CQDs@TMP195

An infrared thermal imaging camera-FLIR ONE Pro was used to record and monitor aqueous solutions of CQDs@TMP195 with different concentrations (0, 75, 125, 175, 200, and 250 µg/ml) under ambient illumination at 808 nm (1.5 W/cm^2, 10 min). The samples with different concentrations were illuminated for 10 min respectively to obtain photothermal images of samples with different concentrations and draw real-time temperature change curves. To further evaluate the photothermal stability of the CQDs@TMP195 solution, the 200 µg/ml of CQDs@TMP195 solution was first irradiated with an 808 nm laser until the solution reached a steady temperature and then cooled to room temperature.

In vitro phototoxicity

Calcein-AM and propidium iodide (PI) co-staining test was performed to monitor the *in vitro* phototherapy efficiency of CQDs. HeLa cells were incubated with different concentrations of CQDs@TMP195 for 4 h and then exposed to 808 nm laser irradiation for 10 min. Afterward, a mixture solution containing 2 µM calcein-AM and 5 µM PI was added, and cells were incubated for 30 min, washed with PBS, and then imaged by fluorescence microscope. CCK8 assay was used to investigate the phototoxicity of CQDs@TMP195.

Repolarization of macrophages phenotype

RAW264.7 cells were planted in 24-well plates at a density of 1×10^5 cells/well and cultured for 24 h. Cells were then treated with 20 ng/ml murine IL-4 for 24 h to obtain M2 phenotype macrophages. Cells were washed with PBS 3 times and cultured with different concentrations of TMP195 for another 24 h. Cells were then stained with antibodies against APC/Cy7-F4/80, PE/Cy7-MHCII, and APC-CD206 and analyzed by flow cytometry.
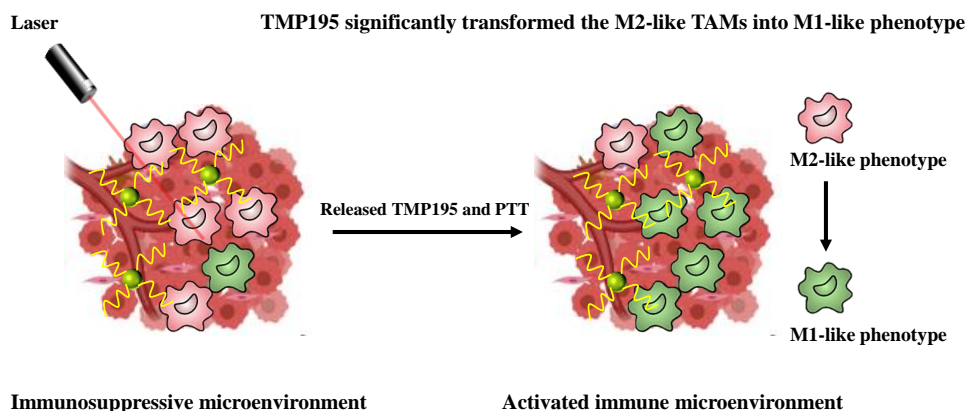
Fig. 1 M2 phenotype TAMs induced to M1 phenotype by CQDs@TMP195 after polarization combined with PTT.

To examine the ability of NPs to repolarize M2 phenotype macrophages into M1 phenotype, RAW264.7 cells were pretreated as described above and incubated with different NPs for 24 h. Then, cells were labeled with the APC/Cy7-F4/80 and PE-CD206 antibodies and detected by a flow cytometer. Moreover, cell supernatants were collected to analyze the levels of IL-2 and IL-10 by enzyme-linked immunosorbent assay (ELISA).

In vivo biocompatibility

To test the potential *in vivo* toxicity, CQDs@TMP195 were administered intravenously to healthy BALB/c mice. Seven days later, the animals were then sacrificed, and major organs were collected. The organs were stored in 4% paraformaldehyde for hematoxylin and eosin (H&E) staining and microscopic observation. Biochemical indexes (alanine aminotransferase-ALT, aspartate aminotransferase-AST, creatinine-CRE, and blood urea nitrogen-BUN) were detected with the corresponding biochemical kits by a blood biochemical auto-analyzer.

Statistical analysis

Data were presented as mean ± SD. The two-tailed unpaired Student's *t*-test was used for statistical analysis between different groups.

RESULTS AND DISCUSSION

Preparation and characterization of CQDs@TMP195

CQDs were synthesized by a facile method using PDA as a carbon source with efficient photothermal effect under 808 nm excitation [27]. Then, the TAMs repolarization agent TMP195 was loaded onto the CQDs to form CQDs@TMP195. The morphologies of CQDs and CQDs@TMP195 were separately characterized by TEM. As shown in Fig. 2A, the CQDs hold a uniformly

spherical structure. The high-resolution TEM (HR-TEM) images presented the crystalline structure of the CQDs with a lattice spacing of 0.21 nm (Fig. 2B), which was consistent with the (100) facet of graphene [28]. The representative TEM image of CQDs@TMP195 also exhibited a highly uniform sphere-like structure (Fig. 2C). The average hydrodynamic sizes of CQDs and CQDs@TMP195 were detected using the dynamic light scattering (DLS) method, and the diameters increased from 4.1 nm of CQDs to 7.7 nm of CQDs@TMP195 (Fig. 2D). In addition, the average surface charge changed from −10.7 mV of CQDs to −5.8 mV of CQDs@TMP195 due to the surface coating with TMP195 (Fig. 2E). When the mass ratio of CQDs@TMP195 was 1:1, the adsorption efficiency and drug loading efficiency of TMP195 were $23.85 \pm 0.93\%$ and $23.69 \pm 1.63\%$, respectively (Fig. 2F). This ratio was used in all the following experiments.

To detect the structural stability of CQDs@TMP195 in physiological conditions, we observed their zeta potential and size changes within 7 days, which showed negligible changes and indicated good structural integrity of CQDs@TMP195 (Fig. 3A,B). This can be compared to a previous report which showed that 3-mercaptopropionic acid-QDs and glutathione-QDs were highly stable in HepG2 cells [29]. Here, further characterization using the UV-vis spectra showed that the CQDs@TMP195 exhibited a broad NIR absorption spectrum from 600 to 900 nm in water (Fig. 3C). Owing to the strong absorption of CQDs@TMP195 in the NIR range, we further investigated their photothermal performance in the NIR region. Under 808 nm laser irradiation, the temperature of CQDs@TMP195 water dispersions showed a dose-dependent manner, and the maximum temperature of 200 µg/ml was around 45 °C, indicating their superior photothermal capability (Fig. 3D). The temperature showed a slight difference after 4 cycles of the laser off/on, proving
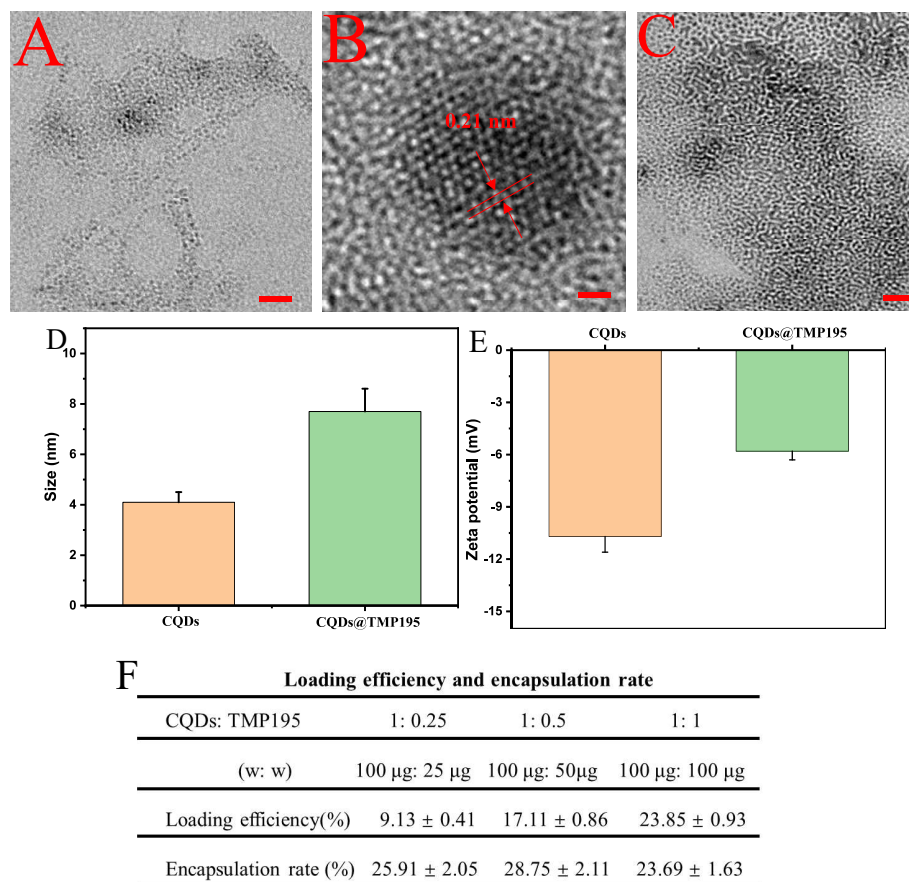
Fig. 2 (A) TEM (scale bar, 50 nm) and (B) HR-TEM (scale bar, 0.5 nm) images of CQDs. (C) TEM image of CQDs@TMP195 (scale bar, 30 nm). (D) Particle sizes of CQDs and CQDs@TMP195. (E) Zeta potential of CQDs and CQDs@TMP195. (F) The loading efficiency and encapsulation rate of CQDs@TMP195.

the high photothermal stability of the CQDs@TMP195 solution (Fig. 3E). Moreover, the temperature change of the CQDs@TMP195 solution in one cycle was exhibited in Fig. 3F, and obvious water vapor droplets on the wall of a sample cell were observed after an irradiation cycle.

In vitro PTT of cancer

The biosafety of CQDs@TMP195 with different concentrations in normal cells was detected using RAW264.7 cells. As shown in Fig. 4A, the cell viability among different groups showed no obvious change and was maintained at high levels, which suggested the good biosafety of CQDs@TMP195 for normal cells. To further assess the intracellular distribution of CQDs@TMP195, a colocalization experiment was conducted using HeLa cells co-stained with CQDs@TMP195 and Lyso-Tracker Red, a commercially available probe for lysosomes [30]. As shown in Fig. 4B, the distribution pattern of CQDs@TMP195 (green) overlapped well with the Lyso-Tracker Red labeled lysosomes within the HeLa cells as yellow dots, indicating the CQDs@TMP195 could accumulate in the lysosomes in living cells.

Subsequently, a CCK8 assay was carried out to quantitatively evaluate the *in vitro* PTT efficacy of the CQDs@TMP195 in HeLa cells [31]. As shown in Fig. 4C, the cell viability sharply decreased with the increasing concentration of CQDs@TMP195 from 100 to 200 µg/ml under 808 nm laser irradiation at 1.5 W/cm^2. This observation confirmed that a high temperature over 46 °C could induce irreversible cellular damage. Moreover, co-staining with calcein-AM and PI fluorescent dyes could selectively label the living and dead cells, respectively. The bright red fluorescence signal from PI dye increased with the increasing concentration of CQDs@TMP195 under an 808 nm laser irradiation (1.5 W/cm^2, 10 min), suggesting the occurrence of dead cells (Fig. 4D). In contrast, no obvious red fluorescence was observed in cells with the absence of CQDs@TMP195. These results suggest that CQDs@TMP195 possesses strong PTT efficiency, which is consistent with the CCK8 assay.
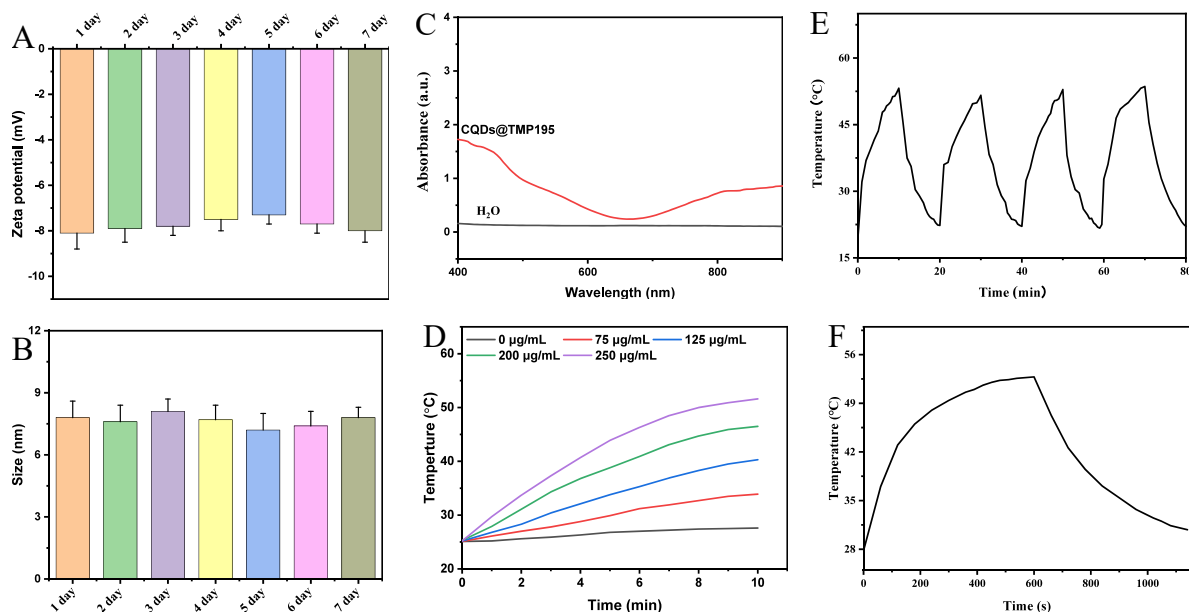
Fig. 3 (A) Zeta potential and (B) size of CQDs@TMP195 stored in PBS for 7 days. (C) UV-vis absorption spectra of water and CQDs@TMP195. (D) Temperature curves of different concentrations of CQDs@TMP195 solutions under 808 nm laser irradiation (1.5 W/cm^2). (E) Temperature variation of the CQDs@TMP195 dispersion (200 μg/ml) with 808 nm laser (1.5 W/cm^2) on and off for 4 cycles. (F) Temperature variation of the CQDs@TMP195 dispersion (200 μg/ml) with 808 nm laser (1.5 W/cm^2) in one irradiation cycle.
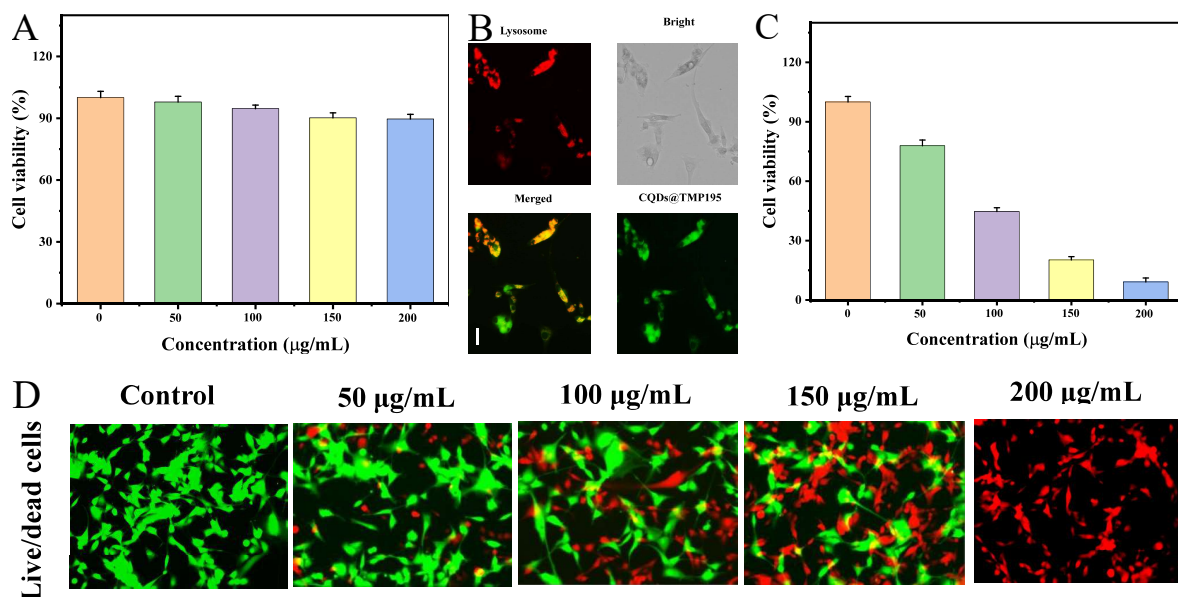

Fig. 4 (A) Cell viability of RAW264.7 incubated with CQDs@TMP195 at various concentrations. (B) Fluorescent microscopy images of HeLa cells with CQDs@TMP195 incubation (scale bar, 20 μm). (C) Cell viability of HeLa cells in a CQDs@TMP195 concentration-dependent manner under an 808 nm laser irradiation for 10 min. (D) *In vitro* PTT therapeutic effect for HeLa cells using a calcein AM/PI co-staining method.

In vitro repolarization of M2 phenotype into M1 phenotype macrophages

The PTT-triggered inflammation recruited many TAMs and stimulated them to polarize into the M2 phenotype, exerting tumor-promoting activity. Compared with the elimination of M2 phenotype TAMs, repolarizing TAMs into the antitumor M1 phenotype would be more attractive [32, 33]. Therefore, we investigated the ability of CQDs@TMP195 in repolarizing the phenotype of TAMs *in vitro*. Firstly, the murine macrophage RAW264.7 cells were pre-polarized into the M2 phenotype through incubation with murine interleukin-4 (IL-4) for 24 h. To optimize the drug concentration, the M2 phenotype RAW264.7 cells were treated with different concentrations of TMP195 for another 24 h, and the percentage of M1 phenotype and M2 phenotype macrophages were analyzed using flow cytometry by measuring the levels of different biomarkers, MHCII+ and CD206+, respectively (Fig. 5A,B). These results showed that the proportion of M1 phenotype macrophages (MHCII+ F4/80+) significantly increased with the increasing concentration of TMP195 treatment while the proportion of M2 phenotype macrophages (CD206+ F4/80+) decreased.

Next, the M2 phenotype RAW264.7 cells were obtained as above and incubated with CQDs, TMP195, CQDs@TMP195, and CQDs@TMP195 + NIR laser irradiation (1.5 W/cm^2, 10 min) for 24 h. As shown in Fig. 5C, the percentage of the M2 phenotype (CD206+ F4/80+) in the CQDs@TMP195 group decreased to 23.3%, while that in the TMP195 group was 19.1%. In addition, the CQDs@TMP195 with an 808 nm laser (1.5 W/cm^2, 10 min) also possessed the ability in decreasing the percentage of M2 phenotype macrophages, indicating the stability of TMP195 under NIR laser irradiation. Besides, cell culture supernatants in control, CQDs, TMP195, CQDs@TMP195, and CQDs@TMP195 + NIR were collected, and the concentrations of IL-2 and IL-10 were detected by using ELISA [34]. As expected, CQDs@TMP195 + NIR treatment significantly enhanced the M1-related cytokine IL-2 but reduced the M2-related inflammatory factor IL-10 (Fig. 5D,E). These results indicated that CQDs@TMP195-generated PTT could repolarize the M2 phenotype into the M1 macrophages and further promote the deteriorative immunosuppressive microenvironment.

In vivo toxicity evaluation

To assess the long-term biosafety of CQDs@TMP195 *in vivo*, heart, liver, spleen, lung, kidney, and serum were collected after 2 weeks of injection. H&E staining assay of the major organs was performed, which showed normal tissue structures without obvious toxicity (Fig. 6A). Moreover, the functions of the liver and kidney were also evaluated. As shown in Fig. 6B–E, the levels of ALT, AST, CRE, and BUN were not significantly

different among all the groups and within the normal reference range. Taken together, the CQDs@TMP195 showed considerable good biosafety *in vivo*.

CONCLUSION

In summary, we have developed a green approach to prepare CQDs@TMP195 under facile and mild reaction conditions. The *in vitro* and *in vivo* toxicity analysis results showed that CQDs@TMP195 had negligible toxicity for normal cells and tissues. The CQDs@TMP195 showed a good photothermal effect under NIR laser irradiation. The application of TMP195 significantly decreased the immunosuppressive M2 phenotype TAM population and increased the tumor-inhibiting M1 phenotype TAM population to potentiate immune activity. Furthermore, the upregulation of MHCII protein on the surface of TAMs demonstrated the facilitation of adaptive immune response. The *in vitro* experiments demonstrated that CQDs@TMP195-generated PTT could offer excellent cancer therapy efficacy under NIR laser irradiation. Thus, this strategy might serve as a more effective combinational method to tackle the post-treatment issue of PTT in the circumstances.

REFERENCES

1. Yuan Z, Lin C, He Y, Tao B, Chen M, Zhang J, Liu P, Cai K (2020) Near-Infrared light-triggered nitric-oxide-enhanced photodynamic therapy and low-temperature photothermal therapy for biofilm elimination. *ACS Nano* **14**, 3546–3562.
2. Liu B, Jiao J, Xu W, Zhang M, Cui P, Guo Z, Deng Y, Chen H, et al (2021) Highly efficient far-red/NIR-absorbing neutral Ir(III) complex micelles for potent photodynamic/photothermal therapy. *Adv Mater* **33**, 2100795.
3. Xu Y, Zhang Y, Li J, An J, Li C, Bai S, Sharma A, Deng G, et al (2020) NIR-II emissive multifunctional AIEgen with single laser-activated synergistic photodynamic/photothermal therapy of cancers and pathogens. *Biomaterials* **259**, 120315.
4. Zhang M, Wu F, Wang W, Shen J, Zhou N, Wu C (2018) Multifunctional nanocomposites for targeted, photothermal, and chemotherapy. *Chem Mater* **31**, 1847–1859.
5. Wen K, Tan H, Peng Q, Chen H, Ma H, Wang L, Peng A, Shi Q, et al (2022) Achieving efficient NIR-II type-I photosensitizers for photodynamic/photothermal therapy upon regulating chalcogen elements. *Adv Mater* **34**, 2108146.
6. Zhang M, Wang W, Mohammadniaei M, Zheng T, Zhang Q, Ashley J, Liu S, Sun Y, et al (2021) Upregulating aggregation-induced-emission nanoparticles with blood-tumor-barrier permeability for precise photothermal eradication of brain tumors and induction of local immune responses. *Adv Mater* **33**, 2008802.
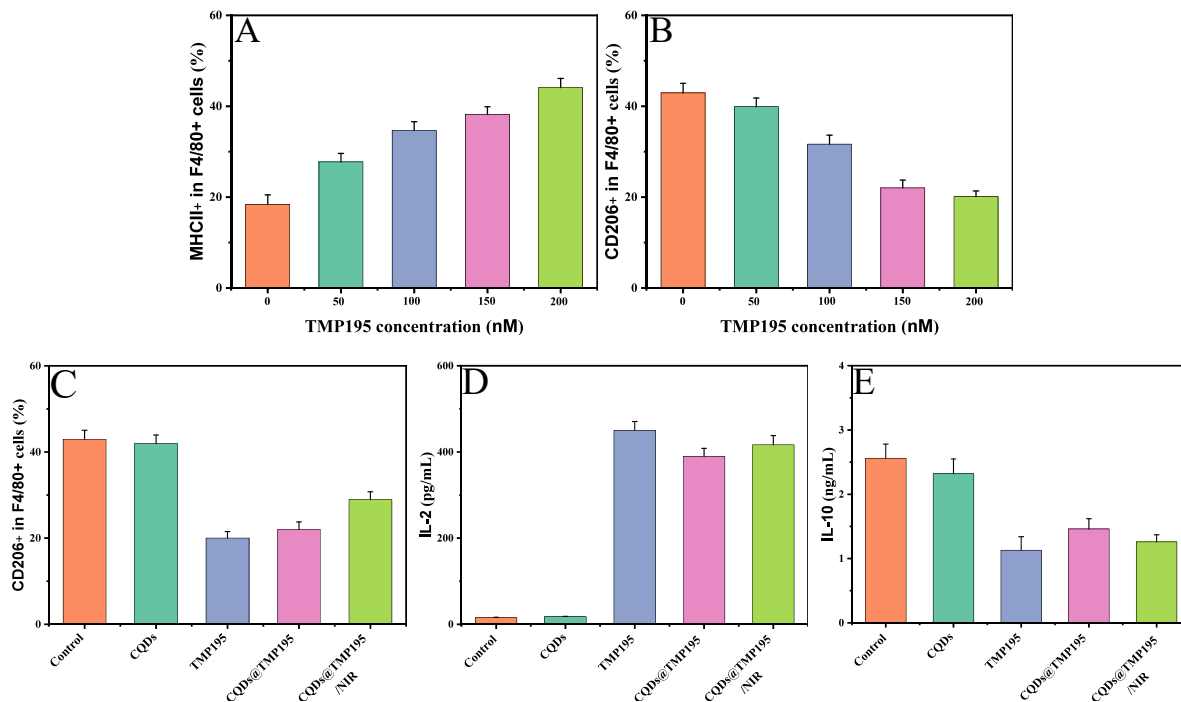
Fig. 5 (A) The percentages of the M1 phenotype (MHCII+ F4/80+) and (B) M2 phenotype (CD206+ F4/80+) were quantitatively analyzed after incubating with TMP195 at different concentrations for 24 h. (C) The percentage of M2 phenotype (CD206+ F4/80+) was quantitatively analyzed after incubating with CQDs, TMP195, CQDs@TMP195, and CQDs@TMP195 under 808 nm laser irradiation for 24 h (with 200 nM of TMP195). Levels of (D) IL-2 and (E) IL-10 in cell supernatants after various treatments were detected by ELISA.
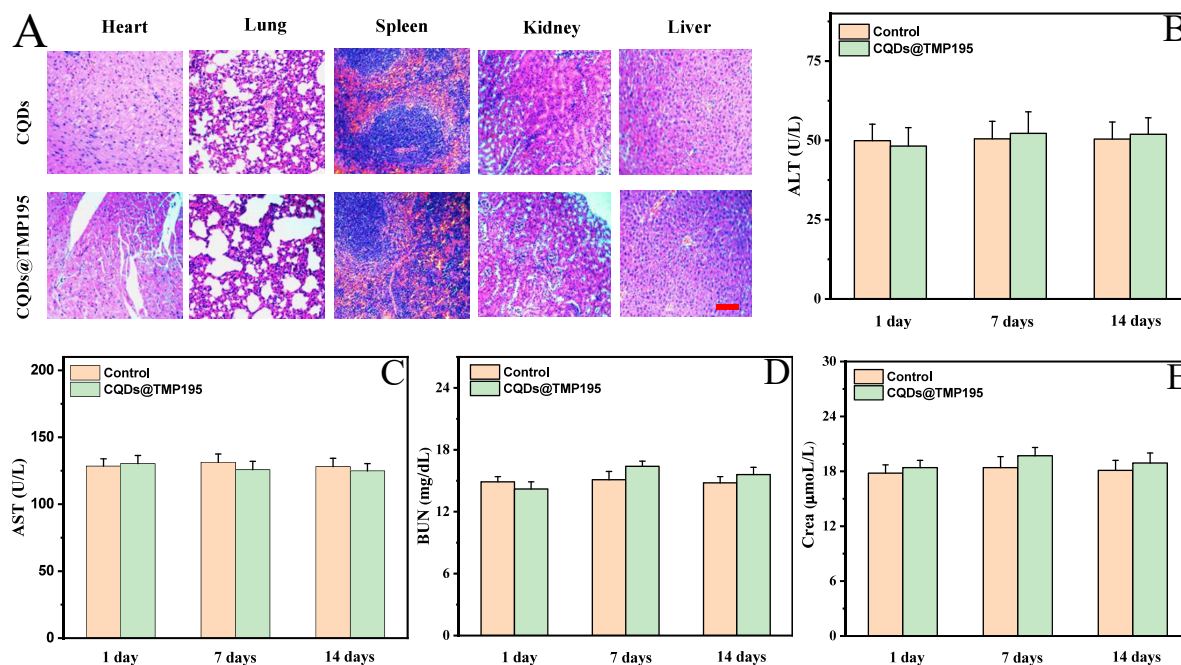

Fig. 6 (A) Major organs were stained with H&E and observed under a microscope (Scale bar, 200 μm). (B–E) Biochemical indexes analysis of liver function (ALT and AST) and kidney function (BUN and Crea).

7. Zhao DL, Chung TS (2018) Applications of carbon quantum dots (CQDs) in membrane technologies: A review. *Water Res* **147**, 43–49.

8. Zhang M, Wang W, Zhou N, Yuan P, Su Y, Shao M, Chi C, Pan F (2017) Near-infrared light triggered phototherapy, in combination with chemotherapy using magnetofluorescent carbon quantum dots for effective cancer treating. *Carbon* **118**, 752–764.

9. Yu H, Huang J, Jiang L, Shi Y, Yi K, Zhang W, Zhang J, Chen H, et al (2020) Enhanced photocatalytic tetracycline degradation using N-CQDs/OV-BiOBr composites: Unraveling the complementary effects between N-CQDs and oxygen vacancy. *Chem Eng J* **402**, 126187.

10. Yao YY, Gedda G, Girma WM, Yen CL, Ling YC, Chang JY (2017) Magnetofluorescent carbon dots derived from crab shell for targeted dual-modality bioimaging and drug delivery. *ACS Appl Mater Interfaces* **9**, 13887–13899.

11. Qiao Y, Luo D, Yu M, Zhang T, Cao X, Zhou Y, Liu Y (2018) A precisely assembled carbon source to synthesize fluorescent carbon quantum dots for sensing probes and bioimaging agents. *Chem Eur J* **24**, 2257–2263.

12. Han C, Zhang X, Wang F, Yu Q, Chen F, Shen D, Yang Z, Wang T, et al (2021) Duplex metal co-doped carbon quantum dots-based drug delivery system with intelligent adjustable size as adjuvant for synergistic cancer therapy. *Carbon* **183**, 789–808.

13. Wei W, Zhang X, Zhang S, Wei G, Su Z (2019) Biomedical and bioactive engineered nanomaterials for targeted tumor photothermal therapy: A review. *Mater Sci Eng C* **104**, 109891.

14. Das RK, Panda S, Bhol CS, Bhutia SK, Mohapatra S (2019) N-doped carbon quantum dot (NCQD)-deposited carbon capsules for synergistic fluorescence imaging and photothermal therapy of oral cancer. *Langmuir* **35**, 15320–15329.

15. Shi X, Meng H, Sun Y, Qu L, Lin Y, Li Z, Du D (2019) Far-red to near-infrared carbon dots: preparation and applications in biotechnology. *Small* **15**, 1901507.

16. Qian Y, Qiao S, Dai Y, Xu G, Dai B, Lu L, Yu X, Luo Q, et al (2017) Molecular-targeted immunotherapeutic strategy for melanoma *via* dual-targeting nanoparticles delivering small interfering RNA to tumor-associated macrophages. *ACS Nano* **11**, 9536–9549.

17. Song M, Liu T, Shi C, Zhang X, Chen X (2016) Bioconjugated manganese dioxide nanoparticles enhance chemotherapy response by priming tumor-associated macrophages toward M1-like phenotype and attenuating tumor hypoxia. *ACS Nano* **10**, 633–647.

18. Rong L, Zhang Y, Li WS, Su Z, Fadhil JI, Zhang C (2019) Iron chelated melanin-like nanoparticles for tumor-associated macrophage repolarization and cancer therapy. *Biomaterials* **225**, 119515.

19. Ovais M, Guo M, Chen C (2019) Tailoring nanomaterials for targeting tumor-associated macrophages. *Adv Mater* **31**, 1808303.

20. Zheng Y, Han Y, Wang T, Liu H, Sun Q, Hu S, Chen J, Li Z (2021) Reprogramming tumor-associated macrophages via ROS-mediated novel mechanism of ultra-small Cu_{2-x} Se nanoparticles to enhance antitumor immunity. *Adv Funct Mater* **32**, 2108971.

21. Nouri F, Raeissadat SA, Eliaspour D, Rayegani SM, Rahimi MS, Movahedi B (2019) Efficacy of high-power laser in alleviating pain and improving function of patients with patellofemoral pain syndrome: a single-blind randomized controlled trial. *J Lasers Med Sci* **10**, 37–43.

22. Zand N, Ataie-Fashtami L, Djavid GE, Fateh M, Alinaghizadeh MR, Fatemi SM, Arbabi-Kalati F (2009) Relieving pain in minor aphthous stomatitis by a single session of non-thermal carbon dioxide laser irradiation. *J Lasers Med Sci* **24**, 515–520.

23. Salimi M, Mosca S, Gardner B, Palombo F, Matousek P, Stone N (2022) Nanoparticle-mediated photothermal therapy limitation in clinical applications regarding pain management. *Nanomaterials* **12**, 922.

24. Stephen ZR, Zhang M (2021) Recent progress in the synergistic combination of nanoparticle-mediated hyperthermia and immunotherapy for treatment of cancer. *Adv Healthc Mater* **10**, 2001415.

25. Cherukula K, Park MS, Sontyana AG, Mathew AP, Vijayan V, Bae WK, Park IK (2019) Role of immunosuppressive microenvironment in acquiring immunotolerance post-photothermal therapy. *J Korean Med Sci* **34**, 272.

26. Yue Y, Li F, Li Y, Wang Y, Guo X, Cheng Z, Li N, Ma X, et al (2021) Biomimetic nanoparticles carrying a repolarization agent of tumor-asociated macrophages for remodeling of the inflammatory microenvironment following photothermal therapy. *ACS Nano* **15**, 15166–15179.

27. Bai Y, Zhang B, Chen L, Lin Z, Zhang X, Ge D, Shi W, Sun Y (2018) Facile one-pot synthesis of polydopamine carbon dots for photothermal therapy. *Nanoscale Res Lett* **13**, 287.

28. Gong J, Zhang Z, Zeng Z, Wang W, Kong L, Liu J, Chen P (2021) Graphene quantum dots assisted exfoliation of atomically-thin 2D materials and as-formed 0D/2D van der Waals heterojunction for HER. *Carbon* **184**, 554–561.

29. Yin J, Zhang J, Chen M, Yin H, Tian J (2022) Reduction of Cd^{2+}/Ag^+-induced toxicity by 3-mercaptopropionic acid-CdSe/ZnS quantum dots and glutathione-CdSe/ZnS quantum dots in human liver cancer cells. *ScienceAsia* **48**, 414–422.

30. Zhang Q, Yang T, Li R, Zou H, Li Y, Guo J, Liu X, Huang C (2018) A functional preservation strategy for the production of highly photoluminescent emerald carbon dots for lysosome targeting and lysosomal pH imaging. *Nanoscale* **10**, 14705–14711.

31. Wang P, Li X, Yao C, Wang W, Zhao M, El-Toni AM, Zhang F (2017) Orthogonal near-infrared upconversion co-regulated site-specific O_2 delivery and photodynamic therapy for hypoxia tumor by using red blood cell microcarriers. *Biomaterials* **125**, 90–100.

32. Deng X, Liang H, Yang W, Shao Z (2020) Polarization and function of tumor-associated macrophages mediate graphene oxide-induced photothermal cancer therapy. *J Photoch and Photobio B* **208**, 111913.

33. Li Y, Xie J, Um W, You DG, Kwon S, Zhang L, Zhu J, Park JH (2020) Sono/photodynamic nanomedicine-elicited cancer immunotherapy. *Adv Funct Mater* **31**, 2008061.

34. Zhang M, Jiang X, Zhang Q, Zheng T, Mohammadniaei M, Wang W, Shen J, Sun Y (2021) Biodegradable polymeric nanoparticles containing an immune checkpoint inhibitor (aPDL1) to locally induce immune responses in the central nervous system. *Adv Funct Mater* **31**, 2102274.